DESIGN AND SIMULATION OF MICROGRID CONTROL BASED WIND POWER GENERATION SYSTEMS USING FUZZY LOGIC CONTROLLER

A.MANJULA

Assistant professor, Anurag Group of Institutions, CVSR College of Engineering

---***---

ABSTRACT: *In this paper a hybrid ac/dc grid architecture that consists of both ac and dc networks connected together by a bidirectional converter is proposed. This paper presents the design of a dc grid-based wind power generation system in a poultry farm. The proposed system allows flexible operation of multiple parallel-connected wind generators by eliminating the need for voltage and frequency synchronization. A control scheme which uses separate controllers for the inverters during grid-connected and islanded operations is proposed. A model predictive control algorithm that offers better transient response with respect to the changes in the operating conditions is proposed for the control of the inverters. To increase the controller's robustness against variations in the operating conditions a fuzzy based controller is introduced the fluctuations of the micro grid are controller with the constant regulated power a separate controller is introduced to the wind turbine to maintain the fixed power to mitigate the vartional errors. Here we are using the fuzzy controller compared to other controllers i.e. The fuzzy controller is the most suitable for the human decision-making mechanism, providing the operation of an electronic system with decisions of experts. To demonstrate the operational capability of the proposed microgrid when it operates connected to and islanded from the distribution grid, and the results obtained are discussed.*

Index Terms—Wind power generation, Fuzzy controller, dc grid, energy management, model predictive control.

I. INTRODUCTION

A dc microgrid based wind farm architecture in which each wind energy conversion unit consisting of a matrix converter, a high frequency transformer and a single-phase ac/dc converter is proposed. However, the proposed architecture increases the system complexity as three stages of conversion are required. In [17], an investigation on the usefulness of the MPC in the control of parallel-connected inverters is conducted. In conventional practices, the control signals are clipped to stay within the constraints, thus the system will operate at the sub-optimal point. Poultry farming is the raising of domesticated birds such as chickens and ducks for the purpose of farming meat or eggs for food. Besides cooling the farms, the wind energy produced by the cooling fans can be harnessed using wind turbines (WTs) to reduce the farms' demand on the grid. The variability of wind speed in wind farms directly depends on the environmental and weather conditions while the wind speed in poultry farms is generally stable as it is generated by constant-speed ventilation fans. Thus, the generation intermittency issues that affect the reliability of electricity supply and power balance are not prevalent in poultry farm wind energy systems.

A dc microgrid based wind farm architecture in which the WTs are clustered into groups of four with each group connected to a converter is proposed. However, with the proposed architecture, the failure of one converter will result in all four WTs of the same group to be out of service. The DERs in dc micro grids are strongly coupled to each other and there must be a minimum level of coordination between the DERs and the controllers..

To regulate the output voltage and the power flow of the inverters commonly adopted control scheme contains an inner voltage and current loop and an external power loop. These areas include improving the robustness of the controllers to topological and parametric uncertainties, and improving the transient response of the controllers.

As the microgrid is required to operate stably in different operating conditions, the deployment of MPC for the control of the inverters offers better transient response with respect to the changes in the operating conditions and ensures a more robust microgrid operation. There are some research works on the implementation of MPC for the control of inverters.

II.SYSTEM DESCRIPTION AND MODELING

System Description

The overall configuration of the proposed dc grid based wind power generation system for the poultry farm is shown in Fig. 1. The system can operate either connected to or islanded from the distribution grid and consists of four 10 kW permanent magnet synchronous generators (PMSGs) which are driven by the variable speed WTs.
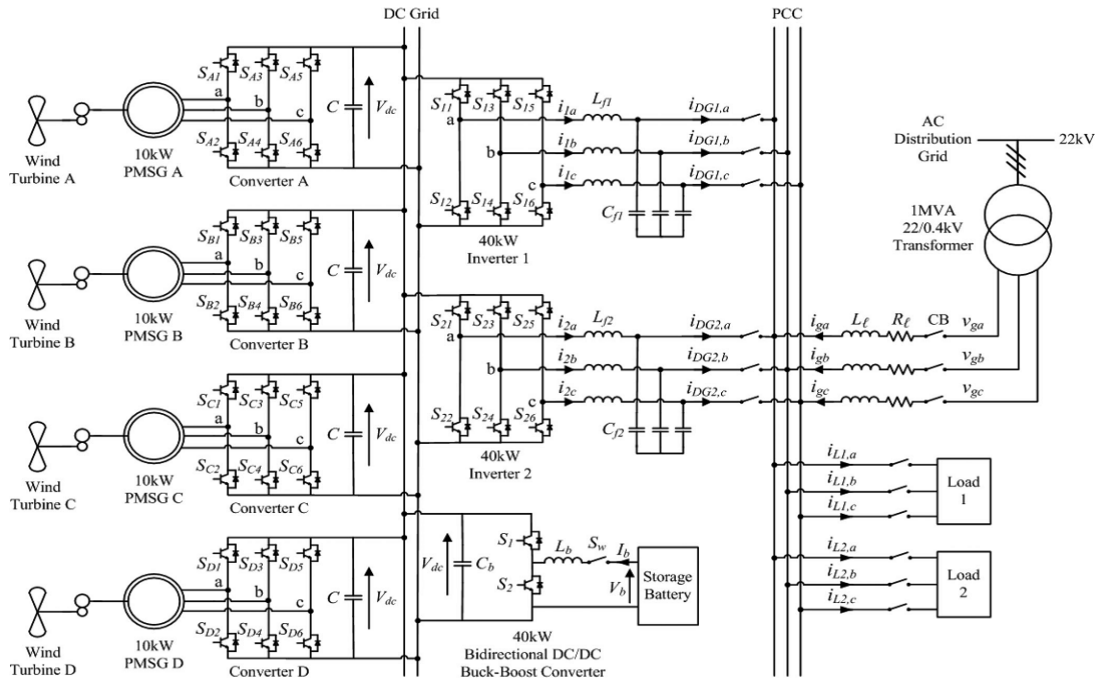
Fig. 1. Overall configuration of the proposed dc grid based wind power generation system in a microgrid.

Instead of using individual inverter at the output of each WG, the use of two inverters between the dc grid and the ac grid is proposed. This architecture minimizes the need to synchronize the frequency, voltage and phase, reduces the need for multiple inverters at the generation side, and provides the flexibility for the plug and play connection of WGs to the dc grid.

The centralized EMS is also responsible for other aspects of power management such as load forecasting, unit commitment, economic dispatch and optimum power flow. During normal operation, the two inverters will share the maximum output from the PMSGs. The maximum power generated by each WT is estimated from the optimal wind power Pwt,opt as follows:

$$P_{wt.opt} = k_{opt}\left(\omega_{r,opt}\right)^3 \qquad (1)$$

$$k_{opt} = \frac{1}{2}C_{P,opt}\rho A\left(\frac{R}{\lambda_{opt}}\right)^3 \qquad (2)$$

$$\omega_{r,opt} = \frac{\lambda_{opt}v}{R} \qquad (3)$$

where k opt is the optimized constant, ωr,opt is the WT speed for optimum power generation, Cp,opt is the optimum power coefficient of the turbine, ρ is the air density, A is the area swept by the rotor blades, λopt is the optimum tip speed ratio, v is the wind speed and R is the radius of the blade. The energy constraints of the SB in the proposed dc grid are determined based on the system-on-a-chip (SOC) limits given by

$$SOC_{min} < SOC \leq SOC_{max} \qquad (4)$$

Although the SOC of the SB cannot be directly measured, it can be determined through the estimation methods. With the use of a dc grid, the impact of fluctuations between power generation and demand can be reduced as the SB can swiftly come online to regulate the voltage at the dc grid.

System Operation

When the microgrid is operating connected to the distribution grid, the WTs in the microgrid are responsible for providing local power support to the loads, thus reducing the burden of power delivered from the grid. The SB can supply for the deficit in real power to maintain the power balance of the microgrid as follows:

$$P_{wt} + P_{sb} = P_{loss} + P_l \qquad (5)$$

where Pwt is the real power generated by the WTs, Psb is the real power supplied by SB which is subjected to the constraint of the SB maximum power Psb,max that can be delivered during discharging and is given by

$$P_{sb} \leq P_{sb,max} \qquad (6)$$

AC/DC Converter Modeling

Fig. 2 shows the power circuit consisting of a PMSG which is connected to an ac/dc voltage source converter. The PMSG is modeled as a balanced three-phase ac voltage source esa,esb,esc with series resistance R s and inductance Ls. The state equations for the PMSG currents isa,isb,isc and the dc output voltage Vdc of the converter can be expressed as follows:

$$L_S \frac{di_s}{dt} = -R_s i_s + e_s - KSV_{dc} \qquad (7)$$

$$C \frac{dV_{dc}}{dt} = i_s^T S - I_{dc} \qquad (8)$$
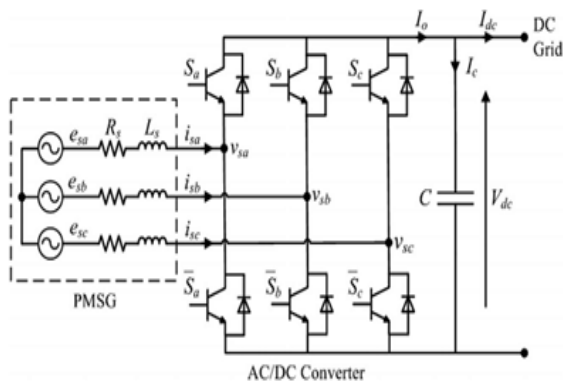
Fig. 2. Power circuit of a PMSG connected to an ac/dc voltage source converter.

DC/AC Inverter Modeling

The two 40 kW three-phase dc/ac inverters which connect the dc grid to the point of common coupling (PCC) are identical, and the single-phase representation of the three-phase dc/ac inverter is shown in Fig. 3.
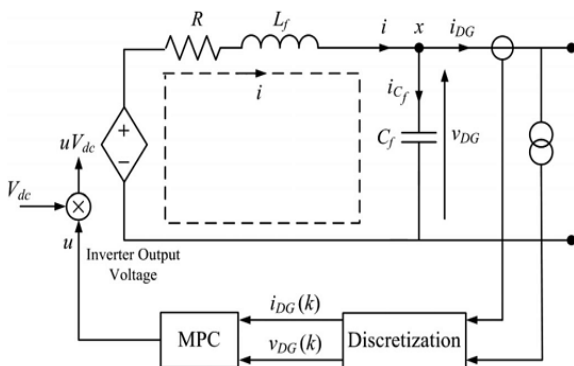
Fig. 3. Single-phase representation of the three-phase dc/ac inverter.

To derive a state-space model for the inverter, Kirchhoff's voltage and current laws are applied to loop i and point x respectively, and the following equations are obtained:

$$L_f \frac{di}{dt} + iR + v_{DG} = uV_{dc} \qquad (9)$$

$$i_{DG} = i - i_{C_f} \qquad (10)$$

where Vdc is the dc grid voltage, u is the control signal, R is the inverter loss, Lf and Cf are the inductance and capacitance of the low-pass (LPF) filter respectively, iDG is the inverter output current, i is the current flowing through Lf , iCf is the current flowing through Cf , and vDG is the inverter output voltage.

During grid-connected operation, the inverters are connected to the distribution grid and are operated in the current control mode (CCM) because the magnitude and the frequency of the output voltage are tied to the grid voltage.

Thus, the discrete state-space equations for the inverter model operating in the CCM can be expressed with sampling time Ts as follows:

$$x_g(k+1) = A_g x_g(k) + B_{g1} v_g(k) + B_{g2} u_g(k) \qquad (11)$$

$$y_g(k) = C_g x_g(k) + D_g v_g(k) \qquad (12)$$

The exogenous input vg(k) can be calculated using state estimation. In this paper, the grid is set as a large power system, which means that the grid voltage is a stable three-phase sinusoidal voltage. Hence, when operating in the CCM, a three-phase sinusoidal signal can be used directly as the exogenous input.

During islanded operation, the inverters will be operated in the voltage control mode (VCM). The voltage of the PCC will be maintained by the inverters when the microgrid is islanded from the grid. As compared to Ts, the rate of change of the inverter output current is much slower. Therefore, the following assumption is made when deriving the state-space equations for the inverter operating in the VCM [33]:

$$\frac{di_{DG}}{dt} = 0 \qquad (13)$$

Based on the above mentioned assumption, the discrete state space equations of the inverter model operating in the VCM can be expressed as follows

$$x_i(k+1) = A_i x_i(k) + B_i u_i(k) \qquad (14)$$

$$y_i(k) = C_i x_i(k) \qquad (15)$$

During islanded operation, the inverters are required to deliver all the available power from the PMSGs to the loads. Therefore, only the inverter output voltage is controlled and the output current is determined from the amount of available power.

CONTROL DESIGN

Control Design for the AC/DC Converter

Fig. 4 shows the configuration of the proposed controller for each ac/dc voltage source converter which is employed to maintain the dc output voltage Vdc of each converter and compensate for any variation in Vdc due to any power imbalance in the dc grid. The power imbalance will induce a voltage error (Vdc ∗ – Vdc) at the dc grid, which is then fed into fuzzy controller to generate a current reference i∗ d for id to track.
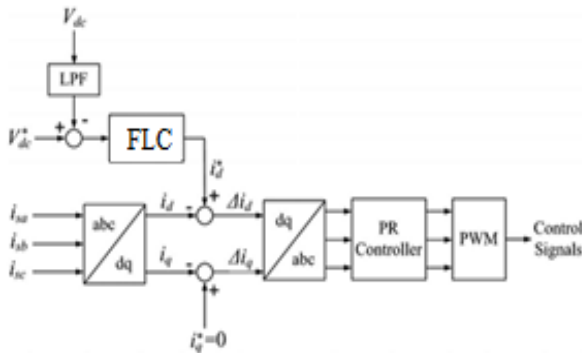
Fig. 4. Configuration of the proposed controller for the ac/dc converter.

Control Design for the DC/AC Inverter

In order for the microgrid to operate in both grid-connected and islanded modes of operation, a model-based controller using MPC is proposed for the control of the inverters. MPC is a model-based controller and adopts a receding horizon approach in which the optimization algorithm will compute a sequence of control actions to minimize the selected objectives for the whole control horizon, but only execute the first control action for the inverter. To derive the control algorithm for the inverters, the state-space equations are transformed into augmented state-space equations by defining the incremental variables in the following format:

$$\Delta\xi(k) = \xi(k) - \xi(k-1) \qquad (16)$$

where ξ represents each variable in the inverter model, such as vDG, iDG, i and u as shown in Fig. 3.

By defining the incremental variables, the augmented statespace model for the inverter model operating in the CCM during grid-connected operation can be expressed as follows:

$$X_g(k+1) = A_{g\_aug}X_g(k) + B_{g1\_aug}V_g(k) + B_{g2\_aug}U_g(k)$$
$$(17)$$

$$Y_g(k) = C_{g\_aug}X_g(k) \qquad (18)$$

Similarly, the augmented state-space model for the inverter model operating in the VCM during islanded operation can be expressed as follows:

$$X_i(k+1) = A_{i\_aug}X_i(k) + B_{i\_aug}U_i(k) \qquad (19)$$
$$Y_i(k) = C_{i\_aug}X_i(k) \qquad (20)$$

For the control of the two augmented models in the CCM and the VCM, the following cost function is solved using quadratic programming in the proposed MPC algorithm [33]:

$$J = (R_s - Y_j)^T(R_s - Y_j) + U_j^T Q U_j \qquad (21)$$

subject to the constraint

$$-1 \le u_j(k) \le 1 \qquad (22)$$

where R s is the set-point matrix, Q is the tuning matrix for the desired closed-loop performance, Yj is the output of either the augmented model in the CCM or VCM (i.e., Yg or Yi), Uj is the control signal of either the augmented model in the CCM or VCM (i.e., Ug or Ui). The first part of the cost function is to compare the output of the augmented model Yj with the reference R s and to ensure that the output tracks the reference with minimum error. After the control signal u is generated by the MPC algorithm, it will be applied to the dc/ac inverter as shown in Fig. 3.

III. FUZZY LOGIC CONTROLLER

In FLC, basic control action is determined by a set of linguistic rules. These rules are determined by the system. Since the numerical variables are converted into linguistic variables, mathematical modeling of the system is not required in FC.
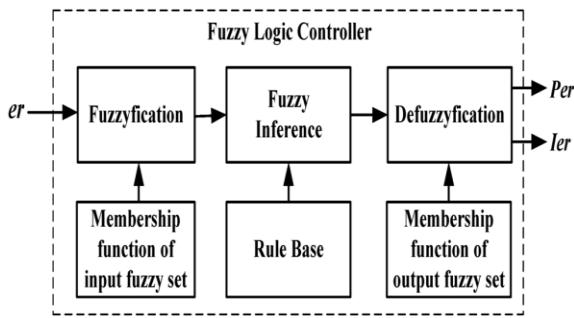
Fig.5.Fuzzy logic controller

The FLC comprises of three parts: fuzzification, interference engine and defuzzification. The FC is characterized as i. seven fuzzy sets for each input and output. ii. Triangular membership functions for simplicity. iii. Fuzzification using continuous universe of discourse. iv. Implication using Madman's, 'min' operator. v. Defuzzification using the height method.

TABLE III: Fuzzy Rules

$\frac{e}{\dot{e}}$	NB	NM	NS	ZE	PS	PM	PB
NB	NB	NB	NB	NB	NM	NS	ZE
NM	NB	NB	NB	NM	NS	ZE	PS
NS	NB	NB	NM	NS	ZE	PS	PM
ZE	NB	NM	NS	ZE	PS	PM	PB
PS	NM	NS	ZE	PS	PM	PB	PB
PM	NS	ZE	PS	PM	PB	PB	PB
PB	ZE	PS	PM	PB	PB	PB	PB

Fuzzification: Membership function values are assigned to the linguistic variables, using seven fuzzy subsets: NB (Negative Big), NM (Negative Medium), NS (Negative Small), ZE (Zero), PS (Positive Small), PM (Positive Medium), and PB (Positive Big). The Partition of fuzzy subsets and the shape of membership CE(k) E(k) function adapt the shape up to appropriate system. The value of input error and change in error are normalized by an input scaling factor.In this system the input scaling factor has been designed such that input values are between -1 and +1. The triangular shape of the membership function of this arrangement presumes that for any particular E(k) input there is only one dominant fuzzy subset. The input error for the FLC is given as

$$E(k) = \frac{P_{ph(k)} - P_{ph(k-1)}}{V_{ph(k)} - V_{ph(k-1)}} \qquad (23)$$

$$CE(k) = E(k) - E(k-1) \qquad (24)$$

Inference Method: Several composition methods such as Max–Min and Max-Dot have been proposed in the literature. In this paper Min method is used. The output

membership function of each rule is given by the minimum operator and maximum operator. Table 1 shows rule base of the FLC.

Defuzzification: As a plant usually requires a non-fuzzy value of control, a defuzzification stage is needed. To compute the output of the FLC, „height" method is used and the FLC output modifies the control output. Further, the output of FLC controls the switch in the inverter. In UPQC, the active power, reactive power, terminal voltage of the line and capacitor voltage are required to be maintained.The set of FC rules are derived from
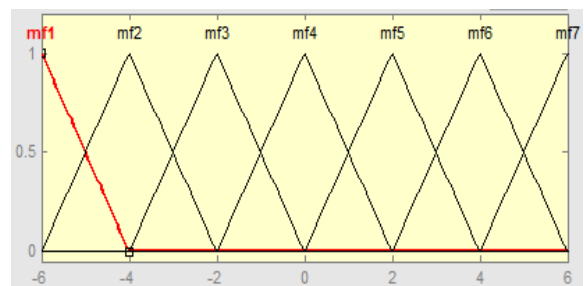
$$u = -[\alpha\,E + (1-\alpha)*C] \qquad (14)$$

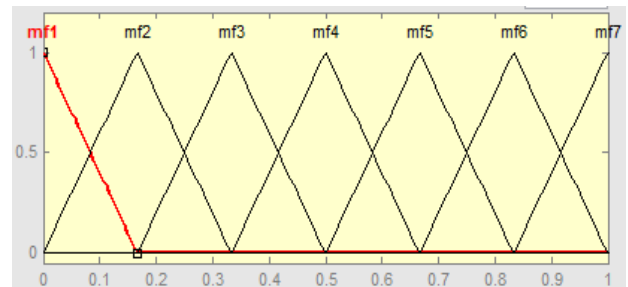Fig: 6 input error as membership functions
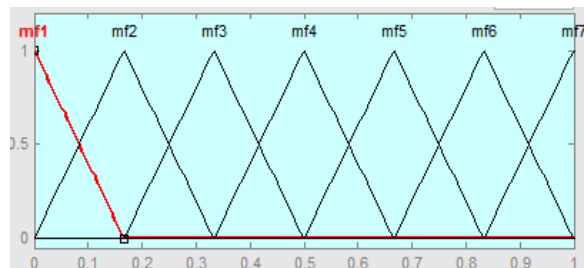

Fig: 7 change as error membership functions

Fig: 8 output variable Membership functions

Where α is self-adjustable factor which can regulate the whole operation. E is the error of the system, C is the change in error and u is the control variable.

SIMULATION RESULT

The simulation model of the proposed dc grid based wind power generation system shown in Fig. 1 is implemented in MATLAB/Simulink. The system parameters are given in Table I.

TABLE I: PARAMETERS OF THE PROPOSED SYSTEM

Parameter	Value
Distribution grid voltage	$v_g = 230$ V (phase)
DC grid voltage	$V_{dc} = 500$ V
PMSG stator impedance	$R_s = 0.2\ \Omega, L_s = 2.4$ mH
Distribution line impedance	$R_\ell = 7.5$ m$\Omega, L_\ell = 25.7\ \mu$H
Inverter LC filter	$L_f = 1.2$ mH, $C_f = 20\ \mu$F
Converter capacitor	$C = 300\ \mu$F
Converter and inverter loss resistance	$R = 1$ mΩ
Load 1 rating	$P_{L1} = 35$ kW, $Q_{L1} = 8$ kVAr
Load 2 rating	$P_{L2} = 25$ kW, $Q_{L2} = 4$ kVAr

Test Case 1: Failure of One Inverter During Grid-Connected Operation

When the microgrid is operating in the grid-connected mode of operation, the proposed wind power generation system will supply power to meet part of the load demand. Under normal operating condition, the total power generated by the PMSGs at the dc grid is converted by inverters 1 and 2 which will share the total power supplied to the loads.
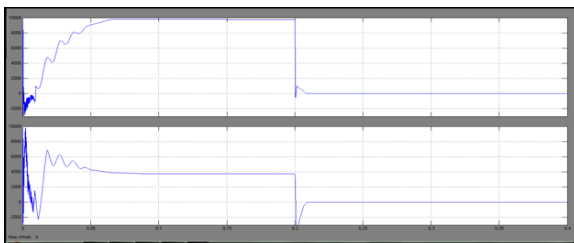
Fig. 9. Real (top) and reactive (bottom) power delivered by inverter 1.
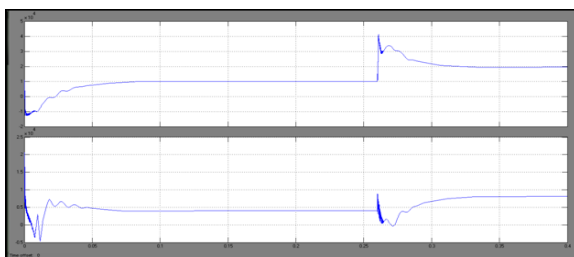
Fig. 10. Real (top) and reactive (bottom) power delivered by inverter 2

Figs. 9 and 10 show the waveforms of the real and reactive power delivered. The remaining real and reactive power that is demanded by the loads is supplied by the grid which is shown in Fig. 11.
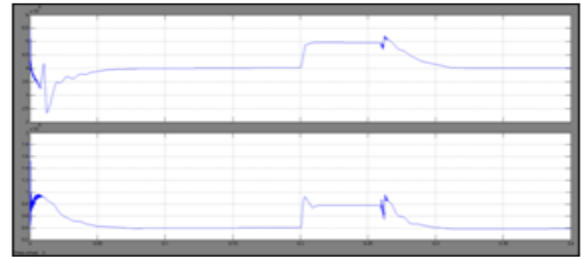

Fig. 11. Real (top) and reactive (bottom) power delivered by the grid.

The total real and reactive power supplied to the loads is about 60 kW and 12 kVAr as shown in the power waveforms of Fig. 12.
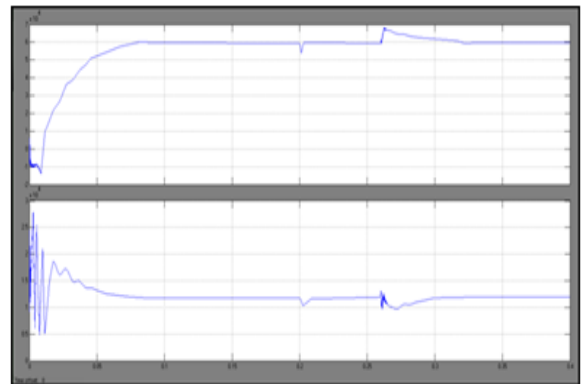

Fig. 12. Real (top) and reactive (bottom) power consumed by the loads.

This undelivered power causes a sudden power surge in the dc grid which corresponds to a voltage rise at t = 0.2 s as shown in Fig. 13.
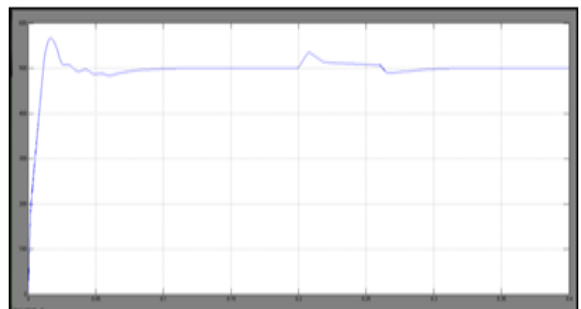

Fig. 13. DC grid voltage.

Test Case 2: Connection of AC/DC Converter During Grid-Connected Operation

As shown in Figs. 14 and 15, each inverter delivers real and reactive power of 7 kW and 4 kVAr to the loads respectively.
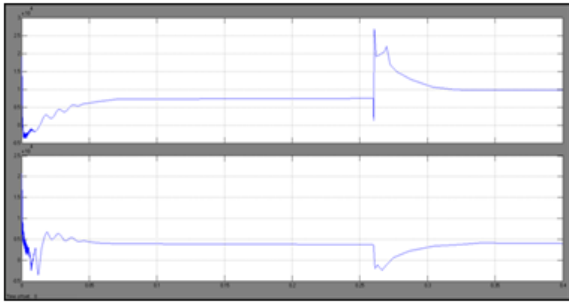

Fig. 14. Real (top) and reactive (bottom) power delivered by inverter 1.
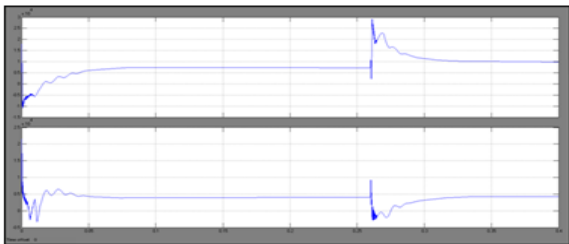

Fig. 15. Real (top) and reactive (bottom) power delivered by inverter 2.

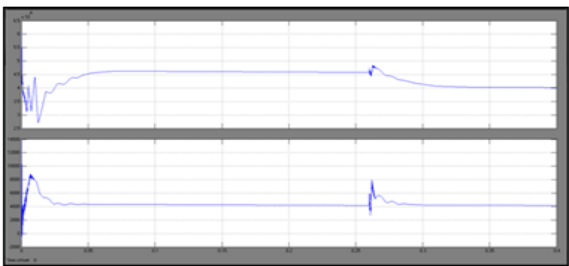The rest of the real and reactive power demand of the loads is supplied by the grid as shown in Fig. 16.

Fig. 16. Real (top) and reactive (bottom) power delivered by the grid.

It can be seen from Fig. 16 that the grid delivers 46 kW of real power and 4 kVAr of reactive power to the loads. This causes a momentarily dip in the dc grid voltage at t = 0.26 s as observed in Fig. 17 which is then restored back to its nominal voltage of 500 V.
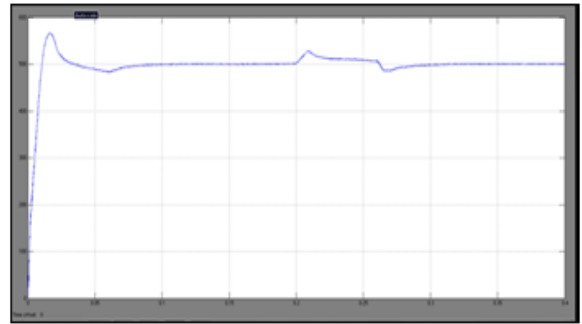

Fig. 17. DC grid voltage.

The grid also simultaneously decreases its supply to 40 kW of real power for 0.26 ≤ t < 0.4 s while its reactive power remains constant at 4 kVAr as shown in Fig. 16.
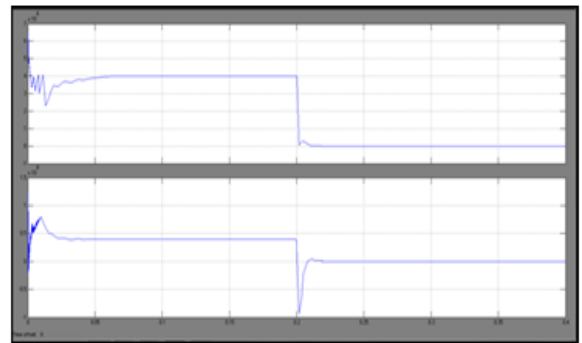

Fig. 18. Real (top) and reactive (bottom) power delivered by the grid.
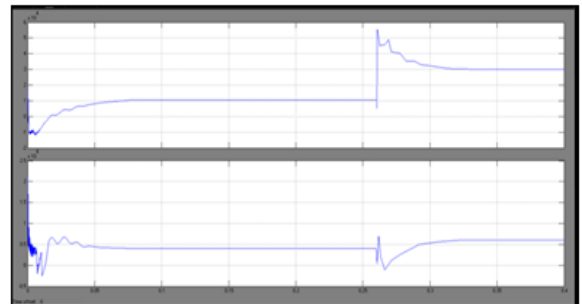

Fig. 19. Real (top) and reactive (bottom) power delivered by inverter 1.

The microgrid is initially operating in the grid-connected mode. It can be seen from Fig. 18 that the CBs fully separate the microgrid from the grid in about half a cycle, resulting in zero real and reactive power supplied by the grid for 0.2 ≤ t < 0.4 s. To maintain the stability of the microgrid, the SB is tasked by the EMS to supply real power of 40 kW at t = 0.26 s as shown in Fig. 21.
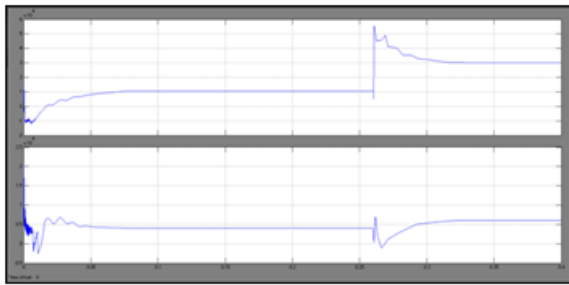
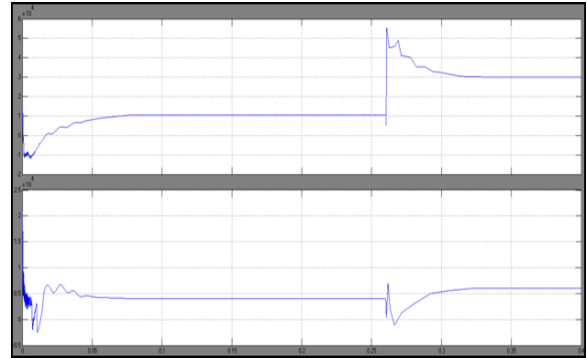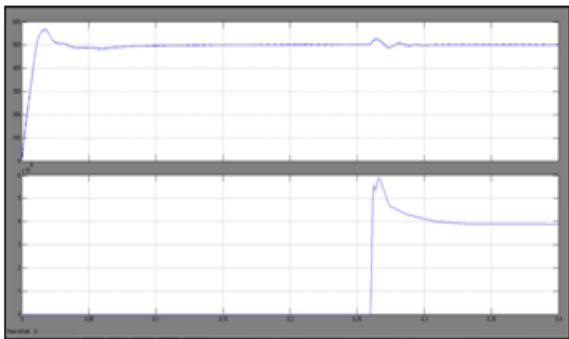Fig. 20. Real (top) and reactive (bottom) power delivered by inverter 2.

Fig. 21. DC grid voltage and Real power delivered by SB.

Fig. 21 shows the dc grid voltage where slight voltage fluctuations are observed at t = 0.26 s.

C. Test Case 3: Islanded Operation

When the microgrid operates islanded from the distribution grid, the total generation from the PMSGs will be insufficient to supply for all the load demand. Under this condition, the SB is required to dispatch the necessary power to ensure that the microgrid continues to operate stably. The third case study shows the microgrid operation when it islands from the grid.
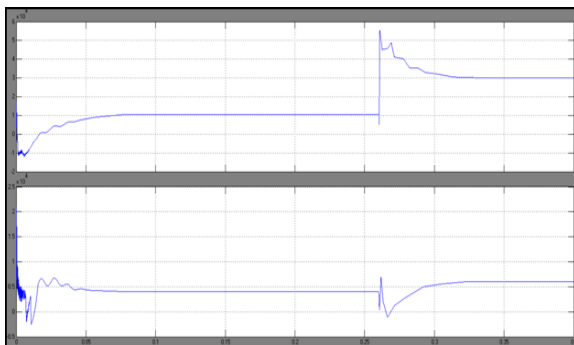

Fig. 22. Real (top) and reactive (bottom) power delivered by inverter 1.
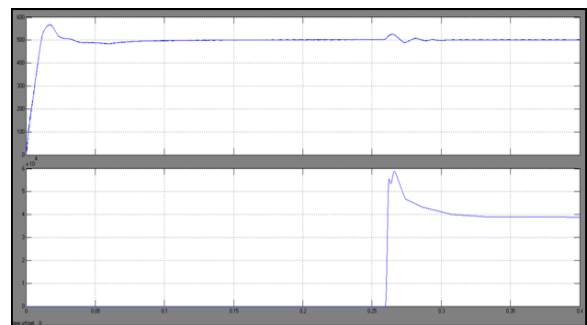

Fig.23. Real (top) and reactive (bottom) power delivered by inverter 2.

Fig. 24. Real power delivered by SB and DC grid voltage.

CONCLUSION

This paper presents the design of a dc grid-based wind power generation system that allows flexible operation of multiple parallel - connected wind generators by eliminating the need for voltage and frequency synchronization. By using the fuzzy controller for a nonlinear system allows for a reduction of uncertain effects in the system control and improve the efficiency. The design of a dc grid based wind power generation system in a microgrid that enables parallel operation of several WGs in a poultry farm has been presented in this paper. comparing to the conventional wind power generation systems, the proposed microgrid architecture eliminates the need for voltage and frequency synchronization, thus allowing the WGs to be switched on or off with minimal disturbances to the microgrid operation. To increase the controller's robustness against variations in the operating conditions a fuzzy based controller is introduced the fluctuations of the micro grid are controller with the constant regulated power a separate controller is introduced to the wind turbine to maintain the fixed power to mitigate the vartional errors. By using the simulation results we can analyze the proposed method.

REFERENCES

[1] M. Czarick and J. Worley, "Wind turbines and tunnel fans," Poultry Housing Tips, vol. 22, no. 7, pp. 1–2, Jun. 2010.

[2] The poultry guide: Environmentally control poultry farm ventilation systems for broiler, layer, breeders and top suppliers.

[3] Livestock and climate change.

[4] Farm Energy: Energy efficient fans for poultry production.

[5] A. Mogstad, M. Molinas, P. Olsen, and R. Nilsen, "A power conversion system for offshore wind parks," in Proc. 34th IEEE Ind. Electron., 2008, pp. 2106–2112

[6] A. Mogstad and M. Molinas, "Power collection and integration on the electric grid from offshore wind parks," in Proc. Nordic Workshop Power Ind. Electron., 2008, pp. 1–8.

[7] D. Jovic, "Offshore wind farm with a series multiterminal CSI HVDC," Elect. Power Syst. Res., vol. 78, no. 4, pp. 747–755, Apr. 2008.

[8] X. Lu, J. M. Guerrero, K. Sun, and J. C Vasquez "An improved droop control method for DC microgrids based on low bandwidth communication with DC bus voltage restoration and enhanced current sharing accuracy," IEEE Trans. Power Electron., vol. 29, no. 4, pp. 1800–1812, Apr. 2014.

[9] T. Dragicevi, J. M. Guerrero, and J. C Vasquez, "A distributed control strategy for coordination of an autonomous LVDC microgrid based on power-line signaling," IEEE Trans. Ind. Electron., vol. 61, no. 7, pp. 3313–3326, Jul. 2014.

[10] N. L. Diaz, T. Dragicevi, J. C. Vasquez, and J. M. Guerrero, "Intelligent distributed generation and storage units for DC microgrids—A new concept on cooperative control without communications beyond droop control," IEEE Trans. Smart Grid, vol. 5, no. 5, pp. 2476–2485, Sep. 2014.